Nonlinear Response of Steel Beams

Dam Safety Office

Report No. DSO-00-01
Department of the Interior
Bureau of Reclamation
December 2000

REPORT DOCUMENTATION PAGE

Form Approved
OMB No. 0704-0188

1. AGENCY USE ONLY *(Leave Blank)*	2. REPORT DATE	3. REPORT TYPE AND DATES COVERED
	December 2000	Final

4. TITLE AND SUBTITLE

Nonlinear Response of Steel Beams

5. FUNDING NUMBERS

6. AUTHOR(S)

Terry Payne

7. PERFORMING ORGANIZATION NAME(S) AND ADDRESS(ES)

Bureau of Reclamation
Technical Service Center
Structural Analysis Group
Denver, Colorado

8. PERFORMING ORGANIZATION REPORT NUMBER

DSO-00-01

9. SPONSORING/MONITORING AGENCY NAME(S) AND ADDRESS(ES)

Same

10. SPONSORING/MONITORING AGENCY REPORT NUMBER

DIBR

11. SUPPLEMENTARY NOTES

12a. DISTRIBUTION/AVAILABILITY STATEMENT

Available from the National Technical Information Service, Operations Division, 5285 Port Royal Road, Springfield, Virginia 22161

12b. DISTRIBUTION CODE

13. ABSTRACT *(Maximum 200 words)*

This paper presents the results preliminary research completed toward the development of plastic failure criteria for components of large fixed wheel spillway gates subjected to seismic loads. Nonlinear finite element analyses were used to model the local buckling mode of failure in plastic hinge regions of beams subjected to cyclic loading. Material testing data from a Stanford University Research Project was used for comparisons to analysis results.

14. SUBJECT TERMS

Nonlinear, Plastic, Buckling, Cyclic, Steel, Hardening, Von Mises Equivalent Stress, Equivalent Plastic Strain, Hystersis Energy

15. NUMBER OF PAGES

75

16. PRICE CODE

17. SECURITY CLASSIFICATION OF REPORT	18. SECURITY CLASSIFICATION OF THIS PAGE	19. SECURITY CLASSIFICATION OF ABSTRACT	20. LIMITATION OF ABSTRACT
UL	UL	UL	UL

Nonlinear Response of Steel Beams

DSO-00-01

by Terry Payne
Structural Analysis Group

December 2000

Contents

Tables and Figures

Table

Figure

Contents - continued

Page

Figure

Contents - continued

Page

Figure

Purpose

The purpose of this study is to determine if the ABAQUS finite element program can be used to accurately model the local buckling mode of failure in plastic hinge regions of beams subjected to cyclic loading, and, if so, to develop practical failure criteria in the plastic range of the material response. This study is a first step in the development of plastic failure criteria for components of large, fixed-wheel spillway gates subjected to seismic loads.

The Stanford University Research Project

Background

The laboratory test data used in this study was obtained from an engineering report entitled "Recommendations for Experimental Studies on the Seismic Behavior of Steel Components and Materials" which was published at Stanford University[1]. The Stanford study was undertaken to identify parameters that would permit an evaluation of deterioration and closeness to failure of a component which is part of a structure that may be subjected to one or several severe earthquakes of random character. The Stanford study included laboratory testing of A36 Structural Steel cantilever beams subjected to cyclic displacement loading at the free end of the beams. There were two failure modes under study in this research project: (1) local buckling in beam flanges and (2) crack propagation. The "B1" specimens were designed so that crack propagation at the weldment was the predominant mode of deterioration. A W4x13 section with a small width to thickness (b/t) ratio for the flange (b/t=11.5) was selected to prevent, as much as possible, the formation of local buckles. The "B2" specimens were designed so that local buckling in the beam flanges was the predominant mode of deterioration. A W6x8.5 section with a flange b/t ratio of 18.9 was selected for the B2 test series. The current Reclamation study focuses on the following three B2 test series: B2-5, B2-6, and B2-8.

Test Specimens and Experimental Setup

Figure 1 shows a sketch of the B2 test setup and connection details. The cantilever beam specimens were connected rigidly to a test frame. A lateral bracing system was provided to prevent lateral torsional buckling of the beams, as shown in figure 1. Loads were applied in a sinusoidal wave form to the free end of the cantilever. All the beams used in the B2 test series were cut from a single piece of hot rolled A36 structural wide flange shape. Measured section properties and computed yield strength and elastic stiffness values for each of the B2 test series specimens are shown in table 1. The overall response of the specimens was recorded through the measurement of applied load, deflection at the free end, and plastic hinge rotation near the fixed end of the beam. The plastic hinge rotation was deduced from pairs of extensometers attached to

the specimens, as shown in figure 2. The free end deflection was used as the control parameter for the input loading history. Strain gages were applied to the flanges at locations where local buckling was anticipated in order to detect the onset of buckling from strain measurements on both sides of the flange. Unfortunately, strain gage measurements were inconsistent and depended on the relative location of the strain gages and the exact location of the local buckle formation. Therefore, the formation, size and shape of local buckles were measured from photos taken at peak deflection points.

Loading Program

The B2 test series consisted of experiments on 10 identical specimens. The Reclamation study used data from three of the constant amplitude cyclic load tests. In these tests, a sinusoidal wave form was used to control the input deflection histories. The average displacement rate in a quarter cycle was selected to define a sine wave with a loading rate of between 0.02 and 0.05 in/sec for all cyclic tests. The tests designated B2-5, B2-8, and B2-6 were included in the Reclamation study. The maximum displacement used in these three tests varied as follows:

(1) Specimen B2-5 Maximum Displacement = 0.765 inches
(2) Specimen B2-8 Maximum Displacement = 1.031 inches
(3) Specimen B2-6 Maximum Displacement = 1.595 inches

Results From the Laboratory Test Series B2 - Local Buckling Study

Table 2 presents a summary of the laboratory testing program for each specimen. In all cyclically loaded test specimens, deterioration due to local buckling was followed by crack propagation and fracture either at the flange weld or at the local buckles. The last column in the table identifies the number of load reversals applied to specimens B2-5 and B2-8 before a through-crack was formed at the weldment and the total number of load reversals to failure. Cracking was observed during the first loading cycle of the specimen B2-6 tests. The number of loading cycles resulting in a through crack for specimen B2-6 was not identified in the Stanford report. Specimen B2-6 cracked through the flange at the buckle rather than in the welds at the support.

The laboratory cyclic load-deflection response of specimens B2-5, B2-6, and B2-8 are shown in figures 3, 4, and 5. Table 3 summarizes the basic response parameters of the B2 specimens subjected to constant amplitude cycling. In this table, P is the peak load at the load reversal point, K is the elastic stiffness at the start of loading and the unloading stiffness, and E is the

hystersis energy which is defined as the area inside the load-displacement hystersis loops. The plastic deflection amplitude ($\Delta\delta_p/2$) shown in the table is the one corresponding to the first excursion.

Cyclic load-rotation curves for specimens B2-6 and B2-8 are shown in figures 6 and 7. The section rotations were calculated for a section located 6 inches from the support. Rotations were calculated from the extension (in the tension flange) and contraction (in the compression flange) measured at the extensometers, according to the following formula:

$$\theta = \tan^{-1}(|\Delta l_g| / (d/2+s))$$

where:

Δl_g is the change in gage length
s is the distance from the gage to the flange surface
d is the beam depth

An average measurement on the tension and compression flanges was assumed to represent the section rotation. The shapes of the load-rotation curves are similar to those of the corresponding load-deflection curves. Minor irregularities in the load-rotation curves were attributed to the localized nature of rotation measurement and the somewhat irregular change in buckle shapes during the cyclic loading.

The only moment-strain diagram provided in the Stanford report was for specimen B2-5 and is shown in figure 8, at the back of this report. The output of pairs of strain gages located on both faces of a flange was only marginally useful detecting the onset of local buckling because the recorded strains are the result of axial deformations due to overall bending and localized bending deformations due to flange buckling.

Photos of the specimen flanges were taken at the peak deflection points during the laboratory testing. Figure 9 shows different buckle shapes for different specimens and compares the stable shapes based on photos taken after the rate of growth in buckle size had decreased considerably. Measurements of buckle sizes (maximum deflection of the flange due to buckling) were taken from the photos. The results of these measurements were plotted against the number of cycles. These plots are shown in figure 10. Figure 11 shows a plot correlating the rate of growth in buckle size and the plastic rotation range $\Delta\theta_p$.

In the laboratory tests, buckling occurred either during the first excursion or, for small deflection amplitudes, after a small number of reversals. Surface cracks developed very early in the load history, in most cases during the first excursion. A noticeable amount of strain hardening was observed during these first few cycles, followed by strain softening as the loading continued. During the loading cycles immediately following the onset of flange buckling, the buckles grew considerably in size, and significant deterioration in the load carrying capacity of the specimens was noticed. Crack growth across the width of the flange was stable during these cycles, with fracture occurring only when the crack propagated across approximately half the flange width. After several cycles, the rate of growth in buckle size decreased continuously, and the rate of deterioration in strength, stiffness, and hystersis energy decreased accordingly. The hystersis energy deterioration plots are shown in figure 36. The final rapid deterioration and subsequent

flange fracture occurred as a result of crack propagation. The load resistance at the stage of fracture had deteriorated to approximately 60 to 70 percent of the undamaged resistance. Final failure during the laboratory tests of all but one of the specimens was caused by fracture of the welded connection at the support. The major crack propagation and fracture in specimen B2-5 occurred at the welded connection along the top flange. Fracture occurred at the welded connection along the bottom flange in specimen B2-8. The fracture of specimen B2-6 occurred at the buckle in the top flange.

ABAQUS STANDARD Analysis

Finite Element Model

Figures 12 through 14 show the ABAQUS model and boundary conditions. The model consists of 1,299 nodes and 1,240 S4R5 shell elements. S4R5 shell elements are four noded, reduced integration, 5 degree of freedom elements. Five integration points were used through the shell thickness at the center of the shell. The finite element mesh of the beam was refined in the region where the plastic hinge was expected to develop. The refined mesh extended 6 inches, measured from the support towards the free end of the beam. Nodes located at the base and top of the support column were fixed. Rollers provided lateral support approximately 4 to 7 inches from the free end of the beam to prevent torsion of the beam. A displacement control boundary condition was applied at all the nodes located on the free end of the beam.

Loading

A single displacement input motion record was created for the ABAQUS analyses. This input motion was a sine wave displacement record with a period of 240 sec and a maximum displacement of 1.0. Load factors of 0.765, 1.031, and 1.595 were applied to the input record for the ABAQUS analysis of specimens B2-5, B2-8, and B2-6, respectively. This resulted in the following loading rates:

(1) Specimen B2-5 Loading Rate = 0.013 inches/second
(2) Specimen B2-8 Loading Rate = 0.017 inches/second
(3) Specimen B2-6 Loading Rate = 0.027 inches/second

Material Property Model

Elastic Material Properties

The elastic material properties define the recoverable part of the strain. The elastic response of the material is modeled linearly. Young's Modulus, Poisson's ratio, and the material density are the only parameters required for the elastic part of the material model. The elastic material properties used in this study were:

$E = 30{,}000{,}000$ psi
$\nu = .27$
$\gamma = 489$ pcf

Nonlinear Isotropic/Kinematic Hardening Model

The nonlinear isotropic/kinematic hardening model was used to model the material response in the plastic range. This material model consists of two components: a nonlinear kinematic hardening component, and a nonlinear isotropic hardening component. There are three methods available for defining the kinematic hardening component of the plasticity: direct parameters; half cycle data, or stabilized cycle data. When the half cycle data method is used, tabulated values of stress and plastic strain from the first half cycle of a unidirectional tension experiment are required, as illustrated in the following figure.

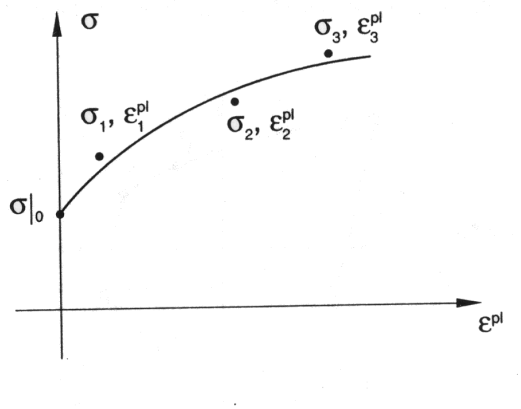

[2]

When Stabilized Cycle Data is used to define the kinematic hardening component, tabulated values of stress and strain from the stabilized cycle of a specimen that has been subjected to symmetric strain cycles are required. A stabilized cycle is obtained by cycling the specimen over a fixed strain range until a steady-state condition is reached. A stabilized cycle is illustrated in the following figure.

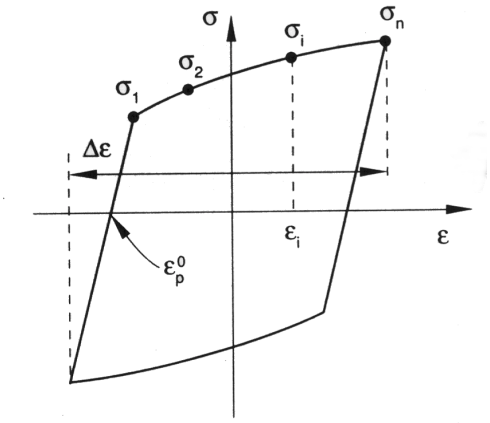

[2]

When the direct parameters method is used to define the kinematic hardening component, the following material parameters are entered directly.

σ_y = the elastic yield stress
C = the initial kinematic hardening modulus
γ = the rate at which the kinematic hardening modulus decreases with increasing plastic deformation.

The direct parameter method of defining the nonlinear kinematic hardening component was used for the ABAQUS analyses in this study because test data, in terms of stress versus strain, was not available. The direct parameter set that most accurately modeled the behavior seen in the laboratory is shown below:

σ_y = 51 ksi
C = 500,000
γ = 50

The isotropic hardening component of the model defines the evolution of the size of the elastic range from cycle to cycle as the following figure illustrates.

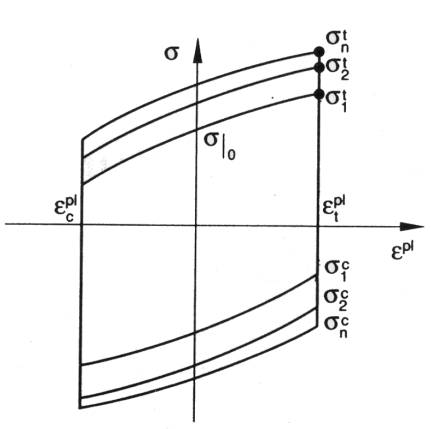

[2]

The isotropic hardening component can be defined in two ways: (1) through direct definition of material parameters or (2) by entering tabulated pairs of equivalent stress to define the size of the elastic range (σ^0) and equivalent plastic strain ($\acute{\varepsilon}^{pl}$) for each loading cycle. The material parameters approach was used in the ABAQUS analyses becuase stress versus strain data were not available. The material parameters which define the isotropic hardening component of the material behavior are as follows:

σ_y = the elastic yield stress
Q = the maximum change in the size of the elastic range
b = the rate at which the size of the elastic range changes as plastic straining develops.

The direct parameter set determined to most accurately model the behavior seen in the laboratory is shown below:

σ_y = 51 ksi
Q = 20,000
b = 10

Analysis Procedure

The capabilities of the ABAQUS nonlinear material model for metals subjected to cyclic loading were evaluated through comparisons of analysis results to data available in the Stanford research paper for the B2 test series. The ABAQUS nonlinear isotropic/kinematic hardening material model was calibrated through comparisons of load-displacement curve values resulting from the ABAQUS analysis and those presented in the Stanford research paper for the B2-8 test. Once a reasonable response match was obtained for the B2-8 specimen, the final material property set was applied in ABAQUS analyses of the B2-5 and B2-6 test series. The material calibration was verified through comparisons of results in terms of load-displacement and load-rotation time histories for all tests for which data was available from the laboratory. Buckle sizes and buckle growth rates for the B2-5, B2-6, and the B2-8 test series were also compared to existing laboratory data. Time history records of equivalent plastic strain, Von Mises equivalent stress,

and the hystersis energy were evaluated relative to the laboratory specimen behavior to determine their potential use as failure criteria.

Analysis Results

Comparisons of Load-Displacement Curves used for Material Property Set Calibration

The load-displacement time history data provided in the Stanford study for the B2-8 test series(peak displacement = 1.031 inches) was used to calibrate the elastic-plastic material model in ABAQUS. The B2-8 Load-Displacement curve is shown in figure 4 of this report. The load and displacement values were scaled from figure 4, tabulated, and then plotted using the ABAQUS post processor so that graphical comparisons could be made. The ABAQUS results in terms of load-displacement curves were generated by summing the reactions at fixed nodes at each time increment and then combining the resulting load time history curve with the displacement time history curve for a node located at the free end of the beam. Material property parameters were adjusted until a reasonable match over most of the loading history was obtained. Figures 15 through 18 show the final ABAQUS load-displacement results plotted against laboratory data for specimen B2-8 for the first 13 loading cycles. The laboratory results are shown in red, while the corresponding ABAQUS results are shown in green. The laboratory and ABAQUS results, in terms of the model's load-displacement response, match very well. In the final cycles of the loading history, the laboratory model was developing cracks through the weld at the connection. The ABAQUS material model used in these analyses does not model cracking, so the load displacement cycles were expected to diverge as cracking progressed.

All the material calibration analyses were completed using ABAQUS STANDARD. The final material set developed through comparisons of load-displacement results for specimen B2-8 were as follows:

Elastic

E = 29,000,000 psi

ν = .27

Plastic

Kinematic Hardening Parameters

Yield Stress	C	γ
51 ksi	500,000	50

Cyclic Hardening Parameters

Yield Stress	Q	b
51 ksi	20,000	10

Comparisons of Load-Displacement Curves Used for Verification of the Material Property Set

The material property set that was developed through analyses of specimen B2-8 was used in the ABAQUS analyses of specimen B2-5 and B2-6. The load conditions were adjusted to represent the load history of the B2-5 test series(peak displacement = 0.765 inches). Figures 19 through 25 show the load-displacement results plotted against laboratory data for 27 loading cycles. The laboratory data are shown in red. Once again, the laboratory and ABAQUS results matched very well over most of the loading history. Next, the load conditions were adjusted to represent the load history of the B2-6 test series(peak displacement = 1.595 inches). Figures 26 through 29 show the load-displacement results plotted against laboratory data for 13 loading cycles. Load-displacement results from the B2-6 analysis do not match the laboratory values nearly as well as the previous two test cases match the lab values. They differ somewhat even in the first cycle of the loading history and continuously diverge in subsequent loading cycles. The maximum displacement used at the free end of the beam was the largest in the B2-6 test case, and the B2-6 test was the only test in which the flange fractured at the location of the flange buckle. Local buckles and cracking developed very early (in the first plastic excursion) in the load history for specimen B2-6. Since these ABAQUS analyses do not model cracking, this divergence in the results seems reasonable.

Comparisons of Load-Rotation Curves Used for Verification of the Material Property Set

Figures 30 and 31 show comparisons of the load-rotation curves for specimens B2-8 and B2-6, respectively. The laboratory data is shown in green. These values were scaled from the test data plots shown in figures 6 and 7. The ABAQUS load-rotation curves were generated using the rotations calculated at a node (node #619) located on the top flange approximately 6 inches from the support. The ABAQUS results from the analysis of specimen B2-8 matched the laboratory results better than results from specimen B2-6 matched the laboratory results, as was the case with the load-displacement results.

Comparisons of Stable Buckle Shape, Size and Growth Rate used for Verification of the Material Property Set

Figures 32, 33, and 34 show isometric and elevation views of the stable buckle shapes resulting from the ABAQUS analyses of specimens B2-5, B2-8, and B2-6, respectively. Each figure also includes a reproduction of the stable buckle shape resulting from the laboratory test, for ease of comparison. The stable buckle shapes produced by the ABAQUS analysis of specimen B2-5 were nearly identical to the stable buckle shapes which resulted from the laboratory experiments. Buckle shapes for specimen B2-8 and B2-6 did not match as well. All the ABAQUS analyses resulted in symmetrical inward buckles on top and bottom flanges. The laboratory tests of specimen B2-8 tended to produce much smaller, outward buckles on the top flange, with larger inward buckles on the lower flange. This may have been the result of imperfections in the test samples. A similar situation exists in the comparisons of stable buckle shapes for specimen B2-6. In this case, the inward buckle shape on the top flange resulting from the laboratory tests

matches the shape produced by the ABAQUS analysis, while the much flatter, outward buckle shape on the bottom flange does not. Again, this could be the result of imperfections in the test samples, or it could represent one effect of the onset of cracking. Cracking occurred at the support on the lower flange during testing of the B2-8 specimens and in the buckle on the top flange for the B2-6 specimens. Cracking on one flange could have affected the development of the buckle on the other flange.

In the Stanford study, the deflections of the flange caused by buckling were measured from the photos of flange buckles and plotted against the number of cycles. These curves were included in figure 10 of this report. The displacement time histories generated in the ABAQUS analyses for a node on the flange where it contacts the web were subtracted from the displacement time histories generated for a node on the free edge of the flange. Both of these nodes were located along the line of maximum deflection of the local buckle. The time values of the resulting time versus buckle size curves were then converted from seconds to the corresponding number of cycles. The ABAQUS Buckle Size versus Number of Cycle curves were then plotted in a MathCadd spread sheet, along with the laboratory values which were scaled from figure 10. These MathCadd plots are shown in figure 35. There are four curves shown on each plot. The two curves shown using only symbols represent the results from the ABAQUS analyses for positive and negative loading on one flange. The other two curves, shown using doted lines, represent the results measured from the laboratory photos for positive and negative loading on one flange. The positive and negative loading curves, when linked, describe the cycling of the flange size as the direction of the applied load oscillates between the positive and negative direction. There was no documentation in the Stanford report to indicate whether the laboratory measurements were taken on the upper or lower flange. The ABAQUS results for Specimens B2-5 represent the buckle growth on the top flange, while the ABAQUS results for Specimens B2-6 and B2-8 represent the buckle growth on the bottom flange. Data were collected from the flange that developed the largest equivalent plastic strains during the analyses. The equivalent plastic strains are discussed in more detail in the following section.

In all cases, the final stable buckle sizes measured in the laboratory were similar to the values calculated by ABAQUS, although their development differed. The maximum buckle size measured from the laboratory photo of Specimen B2-5 was .36 inch, while the maximum buckle size resulting from the ABAQUS analysis of Specimen B2-5 was .41 inch. The maximum buckle size measured from the laboratory photo of Specimen B2-6 was .82 inch, while the maximum buckle size resulting from the ABAQUS analysis of Specimen B2-6 was .86 inch. The maximum buckle size measured from the laboratory photo of Specimen B2-8 was .64 inch, while the maximum buckle size resulting from the ABAQUS analysis of Specimen B2-6 was .77 inch. In the case of the Specimen B2-5 laboratory experiment, the buckle was larger during the negative loading for the first 14 cycles, but then this trend was reversed, such that the larger buckle size developed during the positive loading for the remainder of the test. The ABAQUS analyses of Specimen B2-5 indicated that the larger buckle sizes consistently developed during positive loading. Both the laboratory and the ABAQUS results indicate that the buckle size during positive and negative loading did not converge within 25 cycles when the low amplitude (.765 inch) cyclic load was applied to Specimen B2-5. This indicates that material response was still in the elastic-plastic range at the buckle location when the cracking failure occurred at the support. In contrast, the ABAQUS curves plotted for the large amplitude(1.595 inch) deflection testing of Specimen B2-6 show a nearly plastic material response at the end of 13 loading cycles. This is evident from the convergence of the ABAQUS curves showing buckle size during

positive and negative loading. This is significant, since Specimen B2-6 was the only test where failure actually occurred at the buckle location. The laboratory data for Specimen B2-6 does not show this convergence, although the laboratory and ABAQUS results are very similar with respect to slopes and magnitudes. Finally, in the case of the Specimen B2-8 laboratory experiment, the buckle was larger during the negative loading for the first 3 cycles, but then this trend was reversed, such that the larger buckle size developed during the positive loading for the remainder of the test. The ABAQUS analyses of Specimen B2-8 indicated that the larger buckle sizes consistently developed during positive loading. Both the laboratory and the ABAQUS results indicate that the buckle size during positive and negative loading does not converge within 15 cycles for the 1.031 inch peak amplitude cyclic loading. Therefore, the material response remains the elastic-plastic range at the buckle location during the first 15 loading cycles.

Evaluation of Equivalent Plastic Strain, Von Mises Equivalent Stress, and Hystersis Energy To Determine Potential Use as Failure Criteria

Von Mises yield criterion is frequently used to determine the yield point (the point at which plastic deformation begins) for isotropic metals. This is a distortional energy criterion. It states that yielding occurs when the distortional strain energy density for a multi axial stress state equals the distortional strain energy density at yield in uniaxial tension. The distortional strain energy density for a multi axial stress state (U_d) is defined as:

$$U_d = \frac{\left[\left(\sigma_{11} - \sigma_{22}\right)^2 + \left(\sigma_{22} - \sigma_{33}\right)^2 + \left(\sigma_{33} - \sigma_{11}\right)^2\right]}{12\,G}$$

Where:

U_d is the distortional strain energy density
σ_{11}, σ_{22}, and σ_{33} are the stress components
G is the shear modulus

At yield under a uniaxial stress state:

$$\sigma_{11} = \sigma,\ \sigma_{22} = \sigma_{33} = 0 \quad \text{and} \quad U_d = \sigma_y^2 / 6G$$

So, according to this yield theory, elastic yield occurs when:

$$\sqrt{\frac{1}{2}\left[\left(\sigma_{11} - \sigma_{22}\right)^2 + \left(\sigma_{22} - \sigma_{33}\right)^2 + \left(\sigma_{33} - \sigma_{11}\right)^2\right]} = \sigma_y$$

where σ_y is the yield stress under uniaxial tension load.

The term

$$\sqrt{\frac{1}{2}\left[\left(\sigma_1-\sigma_2\right)^2+\left(\sigma_2-\sigma_3\right)^2+\left(\sigma_3-\sigma_1\right)^2\right]}$$

or

$$\sigma_{eq}=\sqrt{\frac{3}{2}\cdot\sigma\sigma}$$

is known as the Von Mises Equivalent Stress (σ_{eq}).

The plastic equivalent strain(ε_{eq}) is similarly defined as

$$\varepsilon_{eq}=\sqrt{\frac{2}{3}\left[\left(\varepsilon_{11}-\varepsilon_{22}\right)^2+\left(\varepsilon_{22}-\varepsilon_{33}\right)^2+\left(\varepsilon_{33}-\varepsilon_{11}\right)^2\right]}$$

or

$$\varepsilon_{eq}=\sqrt{\frac{3}{2}\cdot\varepsilon\varepsilon}$$

The equivalent plastic strain and Von Mises Equivalent Stress are related as follows:

$$\phi=\frac{3}{2}\cdot\frac{\varepsilon_{EQ}}{\sigma_{EQ}}$$

Where ϕ is a variable factor of proportionality. ϕ is not a constant. Figure 37 illustrates the variable nature of the factor of proportionality. Figure 37 shows time history plot of the factor of proportionality versus time resulting from the analysis of Specimen B2-8 for 15 elements along the bottom flange. Figure 38 show the location of these elements. Values of Von Mises Equivalent Stress and Equivalent Plastic Strain were generated and output at the centroid of these elements from the ABAQUS analyses. [3] [4]

Hystersis energy plots were generated in ABAQUS by generating stress versus time and strain versus time curves and then combining them to create stress-strain curves for the duration of the loading history. The stresses and strains used for these plots were total stress and total strain at the centroid of flange elements oriented along the longitudinal axis of the beam (axis #1, see figure 38). These stress-strain hystersis curves (figures 41, 45, & 50) were then integrated to calculate the area within the hystersis curves. The hystersis energy plots shown in figure 36 resulted from integration of the load-displacement curves generated during the laboratory

experiments. The hystersis energy plots shown in figures 42, 46, and 51 resulted for the integration of stress-strain curves generated from the ABAQUS analyses.

Specimen B2-8 .—Figure 39 shows the time history plots of Von Mises equivalent stresses generated by the ABAQUS analysis of Specimen B2-8 for fifteen elements on the bottom flange. Figure 38 shows the location of these elements. The material model used in these analyses specifies an initial yield stress of 51 ksi, with a 20 ksi maximum increase in the elastic yield due to isotropic hardening. The same material model was used for all specimens (B2-5, B2-6, and B2-8). Figure 39 shows Von Mises stresses versus time, with time in seconds. There are 240 seconds per loading cycle, where one cycle consists of two load reversals. According to Von Mises criterion, the steel should be considered to be in the plastic loading range if the Von Mises stress exceeds 51 ksi during the first cycle. During subsequent loading cycles, the elastic yield point, and therefore the critical Von Mises stress, would vary between 51 ksi and 71 ksi.

The Von Mises stress in the elements at, or immediately surrounding, the local buckle rose to approximately 67 ksi within four or five cycles and remained nearly constant throughout the rest of the loading history. Elements located farther away from the buckle reached their maximum Von Mises stress within the first four or five cycles, followed by a significant decrease in the Von Mises stress level throughout the remainder of the loading history. Elements 1041 through 1045 are located farthest from the support, in the coarse mesh region. The first three of these elements exceeded 51 ksi early in the loading history and then dropped back into the elastic range, while the Von Mises stress in the last two elements (elements 1044 & 1045) never exceeded 51 ksi. Results from these last two elements were useful for comparisons, since the stress levels in these elements remained in the elastic range throughout the loading history.

Figure 40 shows the equivalent plastic strain time history plots for the same 15 elements from the ABAQUS analysis of Specimen B2-8. These plots show the equivalent plastic strain steadily increasing in the elements that form the local buckle. A maximum equivalent plastic strain of 3.7 in/in occurs at the center of the buckle (element 740). In elements farther from the buckle the equivalent plastic strain reaches a peak value within a few loading cycles and then remains constant. The equivalent plastic strain values in the coarse mesh elements remain very low ($\approx$.02 in/in). They reach this peak within two loading cycles and then remain constant. The last two elements (elements 1044 & 1045) never develop any equivalent plastic strain.

Figure 41 shows the hystersis loops for elements 737, 740, 743, and 746. These four elements are shown in red on figure 38. Element 740 is located at the center of the local buckle on the bottom flange. The hystersis loop for element 737 (located next to the support) indicates that this element is in the plastic range for most of the loading history. The hystersis loops do flatten out at the end of the loading history, with a shift in the tensile (+) direction indicating that the element behavior returns to the elastic range, with some permanent deformation (elongation). The hardening followed by softening material response is evident in the increase and subsequent decrease in stress at points of load reversal. The hystersis loops for element 740, which is located at the center of the local buckle, indicate that this element remains in the plastic range throughout the loading history. The initial isotropic hardening was followed by gradual softening, but in this element, the initial softening was followed by a second period of hardening and then softening. The hystersis loops continued to increase in area as the loading continued, with a definite shift in the compressive(-) direction corresponding to the permanent deformation (compression) which

developed at the center of the buckle. The hystersis loops for the last two elements also indicate plastic behavior early in the loading history. The hystersis loops for the element farthest from the support (element 746) flatten out after five or six loading cycles, indicating a return to the elastic range, in this case without developing any permanent deformation.

Figure 41 shows the hystersis energy expended during each loading cycle for these four elements. These points were developed from the integration of the hystersis curves. The area values have been broken down to the area for each cycle and then normalized using the maximum value for each curve. For three of the four elements, the hystersis energy reaches a maximum value within four cycles, followed by a rapid deterioration of the energy level. The hystersis energy level approaches zero as the number of cycles increases. The exception occurs for the element within the local buckle. For this element (element 740), the hystersis energy gradually increases, reaching its peak at 22 cycles. In the laboratory experiments for Specimen B2-8, the first through crack developed in the weld at the support on the bottom flange at 22 cycles. Final failure was the result of this crack propagating from the center of the flange outward to each edge at 28 cycles. The hystersis energy curves generated in the laboratory (figure 36) were based on load-displacement response of the entire model. These curves were very similar to the hystersis curves generated from the ABAQUS analysis for elements sufficiently removed from the local buckling region.

Specimen B2-6.—Figure 43 shows the time history plots of Von Mises equivalent stresses generated by the ABAQUS analysis of Specimen B2-6 for 15 elements on the bottom flange. Figure 38 shows the location of these elements. The Von Mises stress in the elements at, or immediately surrounding, the buckle rose to approximately 67 ksi within two or three cycles and remained nearly constant throughout the rest of the loading history. This is the same behavior seen in elements near, or within, the buckle of Specimen B2-8, except the maximum values were reached in fewer cycles. This seems reasonable, since the loading amplitude was larger in the B2-6 analysis than in the B2-8 analysis. The Von Mises stress in elements farther away from the local buckle also reach a peak value within two to three cycles, but then they gradually decrease throughout the remainder of the loading history rather than remaining constant. The Von Mises stress in the two elements farthest from the buckle (elements 1044 and 1045) never exceeded 51 ksi.

Figure 44 shows the equivalent plastic strain time history plots for the same 15 elements from the ABAQUS analysis of Specimen B2-6. These plots show the equivalent plastic strain steadily increasing in element 740, which is located at the center of the buckle in the bottom flange. A maximum equivalent plastic strain of 5.4 in/in occurred in this element. In the B2-6 analysis, the equivalent plastic strain in the adjacent two elements (which are located within the buckle) gradually increased, leveling off at approximately 2.0 in/in at the end of the loading history. In elements farther away from the buckle, the equivalent plastic strain reached a peak value within two or three loading cycles and then remained constant. The equivalent plastic strain values in the coarse mesh elements remained very low ($\approx$.02 in/in). They reached this peak within two loading cycles and then remained constant. The last two elements (elements 1044 and 1045) never developed any equivalent plastic strain.

Figure 45 shows the hystersis loops for elements 737, 740, 743, and 746. The hystersis loop for element 737 (located next to the support) indicates that this element is in the plastic range for

four or five loading cycles, then the hystersis loops flatten, indicating a return to the elastic range with some permanent deformation (elongation). The hystersis loops for element 740, which is located at the center of the local buckle, indicate that this element remains in the plastic range throughout the loading history. Isotropic hardening was evident during the first three cycles, followed by slight softening for a couple of cycles. The hystersis loops continue to increase in area as the loading continues, with a definite shift in the compressive (-) direction, corresponding to the permanent deformation (compression) which developed at the center of the buckle. The hystersis loops for the last two elements also indicate plastic behavior early in the loading history. The hystersis loops for both elements tend to flatten after five or six loading cycles, although the material behavior stays in the plastic range.

Figure 46 shows the hystersis energy expended during each loading cycle for four of these elements. In three out of the four elements, the hystersis energy reaches a maximum value during the first cycle, followed by rapid deterioration of the energy level, approaching zero as the number of cycles increases. The exception occurs for element 740, which is located within the local buckle. For this element, the hystersis energy gradually increases, reaching its peak at 8 cycles. In the laboratory experiments for Specimen B2-6, cracking developed in the flange at the center of the buckle. The Stanford report states that cracking began during the first loading cycle. But it does not indicate the number of cycles require to develop a through crack. The load-displacement curves for the B2-6 laboratory test show that the test continued for 43 cycles. The ABAQUS analysis of Specimen B2-6 failed to converge after 14 loading cycles.

Specimen B2-5.—Figure 48 shows the time history plots of Von Mises equivalent stresses generated by the ABAQUS analysis of Specimen B2-5 for 15 elements on the top flange. Results were plotted for elements along the top flange from the B2-5 analysis because the equivalent plastic strains were highest on the top flange. Figure 47 shows the location of these elements. The Von Mises stress in the elements at, or immediately surrounding, the buckle rose to approximately 63 ksi in the first loading cycle and then gradually increased to 66.7 ksi over the rest of the loading history. The ABAQUS analyses of all three specimens reached a maximum value of approximately 67 ksi at elements within the buckle. The Von Mises stresses at elements farther away from the local buckle tend to reach their peak values during the first 10 loading cycles and then gradually decrease in value throughout the remainder of the loading history. This response is similar to the results seen in the B2-8 and B2-6 analyses, except that it took a few more cycles to reach the maximum values. This also seems reasonable, since the loading displacement amplitude was significantly lower and the loading rate was slower for the Specimen B2-5 tests. Elements 861 through 865 were located farthest from the support, in the coarse mesh region. The first three of these elements exceeded 51 ksi during the first 10 loading cycles and then drop back into the elastic range. The Von Mises stress in the last two elements (elements 864 & 865) never exceeded 51 ksi.

Figure 49 shows the equivalent plastic strain time history plots for the same 15 elements from the ABAQUS analysis of Specimen B2-5. These plots show the equivalent plastic strain steadily increasing in elements within or adjacent to the local buckle in the top flange. A maximum equivalent plastic strain of 1.5 in/in occurred in this element (566), located at the center of the buckle. In elements farther away from the buckle, the equivalent plastic strain reaches a peak value within 8 to 10 loading cycles and then remains constant. The equivalent plastic strain values in the coarse mesh elements remain very low (≈.02 in/in). They reach this peak within

two loading cycles and then remain constant. The last two elements (elements 864 and 865) never develop any equivalent plastic strain.

Figure 50 shows the hystersis loops for elements 563, 566, 569, and 572. The hystersis loops for element 563 (located next to the support) indicate that this element is in the plastic range throughout the loading history, with some permanent deformation (elongation). The hystersis loops for element 566, which is located at the center of the local buckle, indicate that this element also remains in the plastic range throughout the loading history. Isotropic hardening was evident during the first three cycles, followed by rapid softening for six or seven cycles, and then very gradual softening for the rest of the loading history. The hystersis loops continue to increase in area as the loading continues, with a definite shift in the compressive (-) direction corresponding to the permanent deformation (compression) which developed at the center of the buckle. The hystersis loops for the last two elements also indicate plastic behavior for most of the loading history. The hystersis loops for element 572 tend to flatten out at the end of the loading history.

Figure 51 shows the hystersis energy expended during each loading cycle for these four elements. The hystersis energy in the element farthest from the buckle reaches a peak value by the second cycle, followed by a rapid deterioration of the energy level, approaching zero as the number of cycles increases. The other two elements located outside of the local buckling region also reach their peak values quickly and then decrease, while the hystersis energy curve for the element within the buckle increases throughout the loading history. In the laboratory experiments for Specimen B2-5, cracking developed in the flange weld at the support in 43 cycles. Final failure was the result of this crack propagating from the center of the flange outward to each edge in approximately 55 loading cycles.

Comparisons of Results from Specimens B2-8, B2-6, and B2-5.—Figures 52, 53, and 54 show the maximum values of Von Mises stress, equivalent plastic strain, and hystersis area at each of 15 elements. In figure 52, it is evident that the peak values of Von Mises stress resulting from the analysis of specimen B2-8, which did fail at the buckle, were not significantly different from those obtained from the other two specimens. Figure 53 does show significant differences in the peak values of equivalent plastic strain in the element within or adjacent to the buckle. The maximum value of equivalent plastic strain from the analysis of specimen B2-6 was 5.4, the maximum value from the analysis of specimen B2-8 was 3.7, and the maximum value from the analysis of specimen B2-5 was 1.5. These maximums occurred at elements in the center of the buckle. In all three cases, these elements experienced permanent deformation, although only specimen B2-6 cracked at this location. This curve also shows that in the case of specimen B2-6, the maximum equivalent plastic strain in the element at the center of the buckle is more than twice that of the two adjacent elements. The maximum values from the other two analyses did not result in such a large gradient in the maximum equivalent plastic strain values approaching the center of the buckle. The same pattern was evident in the maximum values of hystersis energy. The maximum value of hystersis energy from the analysis of specimen B2-6 was 25,500, the maximum value from the analysis of specimen B2-8 was 7,970, and the maximum value from the analysis of specimen B2-5 was 2,154. Elements which experienced no permanent deformation experienced equivalent plastic strains of less than .5 in/in and hystersis energies of less than 4,000 in^2.

Conclusions

The ABAQUS finite element program can be used to accurately model local buckling mode of failure in plastic hinge regions of beams subjected to cyclic loading. The results of this study indicate that the global response of the model in terms of displacement and rotation determined by the ABAQUS program match the laboratory results very well. The program also accurately modeled the size and location of the local buckles. While this material model does not directly model cracking of the beam, it did indicate that cracking had occurred in the local buckle of specimen B2-6 when the analysis failed to converge after 13 loading cycles. The steep gradient in the equivalent plastic strain in the elements in and adjacent to the center of the buckle was also an indication that cracking would occur at this location. It appears that the Von Mises stress level is not particularly useful as an indicator of plastic failure. It can be useful in determining the elastic yield point with isotropic and kinematic hardening effects included, but it does not seem useful as a practical failure criteria in the plastic loading range. The equivalent plastic strain, on the other hand, may very well be useful as a failure criteria in the plastic range. It was evident that elements experiencing equivalent plastic strains less than .5 in/in exhibited no permanent deformation, while elements experiencing equivalent plastic strains between .5 in/in and 3 in/in will exhibit permanent deformation, but fracture of the flange at the buckle will not occur. Levels of equivalent plastic strain greater than 3 in/in combined with a large change in equivalent plastic strain level between adjacent elements indicates that fracture of the flange will occur. Hystersis energy could also be useful as an indicator of failure in the plastic range. In this case, levels of hystersis energy of less than 400 in^2 would indicate that no permanent deformation would result. At levels of hystersis energy between 4,000 in^2 and 8,000 in^2, permanent deformation could be expected, but not fracture. Levels of hystersis energy greater than 8,000 in^2, combined with a large change in the hystersis energy between adjacent elements, would indicate that fracture of the flange would be likely to occur.

References

1. Krawinkler, H., M. Zohrei, B. Lashkari-Iravani, N. G. Cofie. September 1983. *Recommendations for Experimental Studies on the Seismic Behavior of Steel Components and Materials*. Stanford University, J.A. Blume Earthquake engineering Center, Stanford, California.

2. Hibbitt, Karlsson & Sorensen, Inc. *ABAQUS/STANDARD User's Manual*, Version 5.8.

3. Spencer, G. C. 1968. *Introduction to Plasticity*. Chapman & Hall LTD.

4. Mase, George. 1970. *Continuum Mechanics*. Schaum's Outline Series. McGraw-Hill, Inc.

MISSION STATEMENTS

The Mission of the Department of the Interior is to protect and provide access to our Nation's natural and cultural heritage and honor our trust responsibilities to tribes.

The mission of the Bureau of Reclamation is to manage, develop, and protect water and related resources in an environmentally and economically sound manner in the interest of the American public.